JOURNAL OF THE AMERICAN CHEMICAL SOCIETY

Article

Redox Active Colloids as Discrete Energy Storage Carriers

Elena C. Montoto, Gavvalapalli Nagarjuna, Jingshu Hui, Mark Burgess, Nina M. Sekerak, Kenneth Hernandez-Burgos, Teng-Sing Wei, Marissa Kneer, Joshua M Grolman, Kevin J. Cheng, Jennifer A. Lewis, Jeffrey S. Moore, and Joaquín Rodríguez-López

J. Am. Chem. Soc., **Just Accepted Manuscript** • DOI: 10.1021/jacs.6b06365 • Publication Date (Web): 15 Sep 2016

Redox Active Colloids as Discrete Energy Storage Carriers

Elena C. Montoto[1,2,‡], Gavvalapalli Nagarjuna[1,2,‡], Jingshu Hui[1,3], Mark Burgess[1,2] , Nina M. Sekerak[2], Kenneth Hernández-Burgos[1,2,4], Teng-Sing Wei[1,5], Marissa Kneer[2], Joshua Grolman[3], Kevin J. Cheng[1,2], Jennifer A. Lewis[1,5], Jeffrey S. Moore [1,2,4,*] and Joaquín Rodríguez-López[1,2,*]

[1]Joint Center for Energy Storage Research.

[2]Department of Chemistry, University of Illinois Urbana-Champaign.

[3]Department of Materials Science and Engineering, University of Illinois Urbana-Champaign.

[4]Beckman Institute of Advanced Science and Technology, University of Illinois at Urbana-Champaign.

[5]Paulson School of Engineering and Applied Sciences, Harvard University.

Supporting Information

ABSTRACT: Versatile and readily available battery materials compatible with a range of electrode configurations and cell designs are desirable for renewable energy storage. Here we report a promising class of materials based on redox active colloids (RACs) that are inherently modular in their design and overcome challenges faced by small-molecule organic materials for battery applications, such as crossover and chemical/morphological stability. RACs are crosslinked polymer spheres, synthesized with uniform diameters between 80 and 800 nm, and exhibit reversible redox activity as single particles, as monolayer films, and in the form of flowable dispersions. Viologen-based RACs display reversible cycling, accessing up to 99% of their capacity and 99 ± 1 % coulombic efficiency over 50 cycles by bulk electrolysis owing to efficient, long-distance intra-particle charge transfer. Ferrocene-based RACs paired with viologen-based RACs cycled efficiently in a non-aqueous redox flow battery employing a simple size-selective separator, thus demonstrating a possible application that benefits from their colloidal dimensions. The unprecedented versatility in RAC synthetic and electrochemical design opens new avenues for energy storage.

INTRODUCTION

There is increasing interest in versatile electrical energy storage materials that readily adapt to different electrode designs as well as capacity and power needs[1-2]. Organic-based redox materials are promising in this regard, with their wide-ranging electrochemical potentials in non-aqueous electrolytes and molecularly tunable properties. However, small organics display pervasive and detrimental material crossover, which limits their long-term use. Here we report on redox active colloids (RACs), a promising class of polymer-based particles that store energy efficiently and reversibly. RACs act as discrete charge carriers that incorporate redox pendants for facile charge transport within a well-defined 3D geometry. These particles are structurally stable, exhibit high charge density, and retain the redox signatures of the constituent monomer, easily varied via organic synthesis.

Combining efficient energy storage with a high degree of morphological control makes RACs a conceptually promising building block deployable in various modalities, including individual particles, well-defined particle films, and redox active dispersions. This versatility addresses several challenges faced by stationary and flow battery materials. Their microscale dimensions dramatically decrease the pervasive and detrimental material crossover observed across separating membranes when small-molecules are used as redox materials.[3-4] Unlike organic nanocrystals which disintegrate during charge/discharge cycling[5-6], RACs retain their morphological integrity due to their cross-linking. In contrast to macromolecules such as dendrimers[7-8], micelles[9] and polymers[10-14], RACs offer a wider range of sizes, spanning from tens to thousands of nanometers.

RAC dispersions, with tunable inter-particle interactions and rheological properties are attractive candidates for emerging non-aqueous flow battery technologies[15-17] that rely on size exclusion rather than ion exchange membranes.[18-19] A major challenge in redox flow batteries is simultaneously decreasing resistive losses due to electrolyte transport through the membrane that separates anolyte and catholyte, while blocking the redox species from crossing over compartments [17-18, 20-21]. Because of the low conductivity of organic electrolytes, this challenge is exacerbated in non-aqueous redox flow batteries (NRFBs). [1, 15-16, 19] We recently demonstrated that inexpensive nanoporous separators enabled a size-selective strategy in NRFBs when using redox active polymers (RAPs) of 8 to 14 nm in diameter as storage media.[12] Nanopores allowed the unimpeded transport of supporting electrolyte, while RAPs largely remained in their half-cell compartment, displaying cross-over values as low as 7%.[12] A polymer-based size-exclusion flow battery has been demonstrated recently.[13] Here, we explore how the larger dimensions attainable with RACs show promise in size-exclusion flow batteries by greatly reducing crossover while preserving the redox properties of its small-molecule constituents. Further, the ability to shuttle charge in discrete units capable of conforming to various electrode designs makes RACs immediately of interest to a broad range of applications in electrochromic devices, redox sensors, and as catalysts, amongst others.[7]

EXPERIMENTAL METHODS

Material Preparation Functionalized RACs (**RACs 1-4**) were prepared from crosslinked colloidal poly(vinylbenzyl chloride) (**xPVBC**) and respective pendants ethyl viologen (**RACs 1-3**) or (dimethylaminomethyl) ferrocene (**RAC 4**). Functionalization involved heating **xPVBC** with the pendant monomer precursor in a mixture of dimethylformamide and tetrahydrofuran followed by purification via centrifugation. Three sizes of viologen RACs were produced and studied: **RACs 1-3** of particle diameters 80 ± 11, 135 ± 12, and 827 ± 71 nm, respectively (Figure 1) as confirmed by scanning electron microscopy (SEM, Figure 1b) in the dry state from the average of 50 particles. Ferrocene RACs (**RAC 4**) were of 88 ± 11 nm by SEM (Figure S4.2). Crosslinked **xPVBC** of varying diameters were synthesized by redox-initiated emulsion polymerization[22] or dispersion polymerization[23] depending on the desired colloid diameter (see Supporting Information). RACs were characterized by elemental analysis, ATR-IR, and UV-Vis spectroscopy. Particle size was determined in both the dry and swollen state. Dynamic Light Scattering (DLS) was used to characterize the swollen size of RACs. Crossover studies were done using a PermGear Side-Bi-Side cell and UV-Vis absorbance (see Supporting Information). All dispersion characterization measurements were done in acetonitrile and concentrations are defined as moles of redox active unit per liter.

Electrochemical Methods All electrochemical measurements were performed on a CHI920D or CHI760 potentiostat and in an O_2 and moisture free environment inside of an Ar-filled drybox. All chemicals, except for synthesized RACs, were purchased from Sigma-Aldrich with the highest available purity and used as received. Unless specified, all transient voltammetric experiments were carried out in a standard three-electrode configuration with either a 12.5 µm radius Pt ultramicroelectrode (UME) or 1 mm radius Pt disk electrode as the working electrode, a non-aqueous Ag/Ag^+ reference electrode (CHI112, 0.1 M AgNO3 in acetonitrile solution), and a Pt wire as counter electrode. Most experiments were carried out in a three-chamber electrochemical cell with 1.0-1.6 µm glass frits. The transient voltammetry of viologen colloids was tested with a 10 mM effective repeating unit concentration for all RACs in 0.1 M LiBF4 in acetonitrile as supporting electrolyte.

RAC monolayers for transient voltammetry were prepared by water-air interface methods onto Au substrates fabricated by e-beam evaporation on Si/SiO_2 substrates (see Supporting Information). Prepared monolayer substrates were then used as working electrodes for transient voltammetry. Circular area (3 mm radius) of the substrate was exposed to supporting electrolyte (0.1 M $LiBF_4$) on a home-made substrate holder.

Scanning Electrochemical Microscopy (SECM) measurements were done using 300 nm radius Pt electrode as the working electrode, a Pt wire as counter electrode and a non-aqueous Ag/Ag^+ reference electrode. The RACs for SECM experiments were deposited onto a glass substrate (see Supporting Information).

Charge storage properties of RAC dispersions were studied by potential-controlled bulk electrolysis (BE). A Pt mesh or carbon felt working electrode were held at a constant overpotential while stirring. Current and charge response over time was recorded. For reduction, the potential was held -150 mV from $E_{1/2}$ and +200-300 mV from $E_{1/2}$ for oxidation. UME voltammograms using 12.5 µm radius Pt UMEs were obtained before and after BE to track steady state limiting currents, confirming complete transformation. A three-compartment cell was used, with the working electrode in the center compartment, and the two lateral compartments occupied by a graphite rod as a counter electrode, and a non-aqueous Ag/Ag^+ reference electrode. The chemical stability of the charged state for **RACs 1-3** was studied by reducing the RACs to the charged state (V^+) via BE and monitoring their absorption spectra over a one week period.

A flow cell made with stainless steel flow fields was used for the NRFB prototype. Porous carbon electrodes (SGL GFA6) were inserted into flow fields as electrode material (4.63 cm^2 active area). Flow fields were separated by Teflon gaskets holding nanoporous separator Celgard 2325. Dispersion was flowed at 5 mL/min on a MasterFlex L/S Digital Drive (HV-07522-30). Dispersions were prepared at 10 mM RAC in 0.1 M $LiBF_4$ in acetonitrile. Galvanostatic cycling was performed on an Arbin BT-2000.

Rheology was performed at 22 °C on a TA Instrument AR-2000EX rheometer using smooth surface finish stainless steel parallel plates (40 mm diameter) with a 500 µm gap height. Measurements of elastic and storage moduli were done at 10 rad/s.

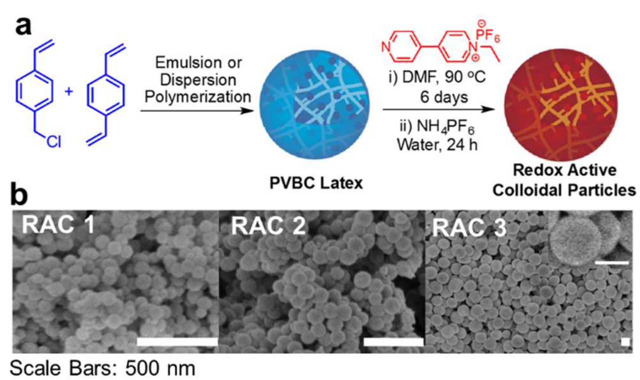

Figure 1. Synthesis and SEM images of redox active colloidal particles (RACs). a. Reaction scheme for the synthesis of polyvinyl benzylchloride and viologen based redox active colloidal particles. **b.** SEM images of the fully-substituted viologen **RACs 1-3** in the dry state: particle diameters of 80 ± 11, 135 ± 12, and 827 ± 71 nm, respectively. Scale bar: 500 nm.

RESULTS AND DISCUSSION

Characterization of RACs 1-3 To illustrate the modularity and simplicity of RAC synthesis, viologen-containing particles were prepared via a modified, post-polymerization protocol[22-23] from ethylviologen and crosslinked poly(vinylbenzyl chloride) (x**PVBC**) latex particles. Percent functionalization for each particle population was nearly 100% as determined by elemental analysis, UV-Vis absorption, and ATR-IR (Tables S2.1-2.2 and S2.5, Figures S2.1-S2.3).

The latter evidenced the complete loss of the 1280 cm^{-1} peak corresponding to the benzyl chloride, accompanied by the limiting growth of the 1650 cm^{-1} peak of the viologen quaternary amine.[12, 24] UV-Vis absorbance peaks were compared to that of the monomer precursors.

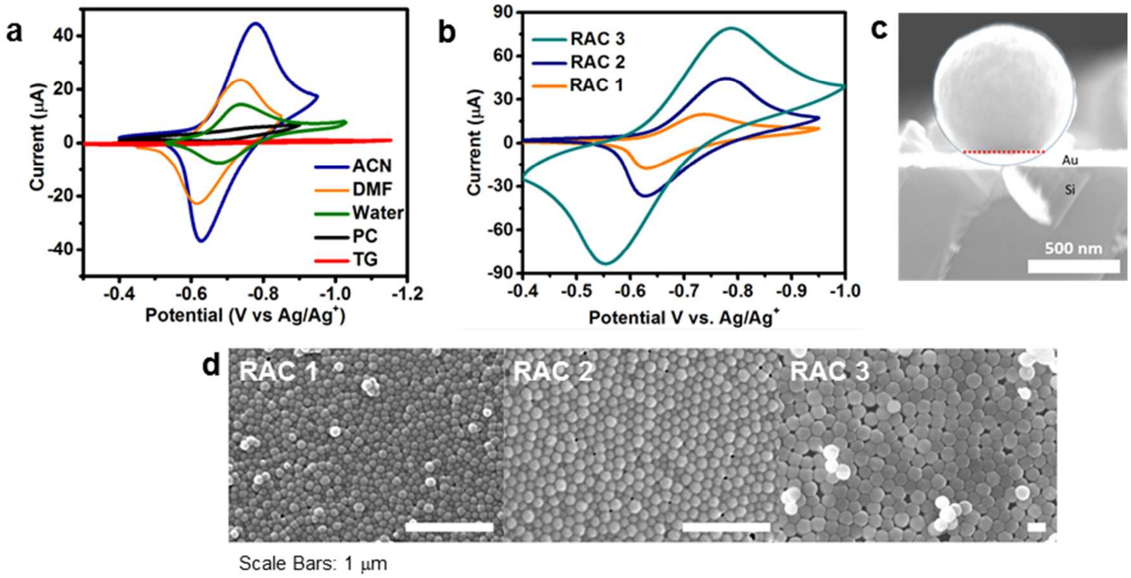

Figure 2. Electrochemical properties of RAC 1-3 monolayers. a. Solvent dependent CVs for **RAC 2** at 20 mV/s in 0.1 M $LiBF_4$ (organic solvents) and 0.1 M KCl (water). Solvents tested were acetonitrile (ACN), *N,N*-dimethylformamide (DMF), propylene carbonate (PC), tetraglyme (TG). **b.** CVs at 20 mV/s for each size RAC in 0.1 M $LiBF_4$ in acetonitrile. **c.** SEM cross-sectional image of **RAC 3** over Au/Si substrate. Scale bar: 500 nm. **d.** SEM images of viologen **RACs 1-3** monolayers prior to testing. Scale bar: 1 μm.

RACs 1-2 display similar absorbance to ethyl viologen at the same repeat unit concentrations, indicating quantitative percent substitution, whereas **RAC 3** exhibited a broadened peak and lower absorbance due to scattering. Notably, the diameter of these particles in acetonitrile, measured by DLS analysis, was 1.7-2.2 times larger than the dry state (Tables S2.3-S2.4), indicating significant swelling. Viologen RACs yielded loadings up to 40 wt% when dispersed in acetonitrile with $LiBF_4$ (corresponding molarity: 0.56 M or 15 Ah/L in 0.1 M $LiBF_4$). The discrete format and high dispersibility of RACs allowed us to probe their redox properties in well-defined films, deposits, and as bulk dispersions.

RAC Monolayer Reactivity Well-ordered monolayers of RACs on Au allowed us to probe intra-particle charge transfer within their films using cyclic voltammetry (CV, Figure 2, S3.1). Monolayer films allowed us to quickly probe the interactions of RACs with various organic solvents and water. CVs indicated marked differences in the charge accessibility as a function of solvent, as evidenced by the different peak heights in Figure 2a, despite similar initial RAC coverage and electrolyte concentration. We observed a correlation between peak height and the inverse of solvent viscosity (Figure S3.1). Viscosity strongly affects diffusion of the supporting electrolyte, suggesting that faster electrolyte transport into the RACs affects their electrochemical performance, although other effects brought by the wettability towards different solvents might still contribute to the observed differences. Acetonitrile allowed the fastest access to charge into the film, thus comparisons of charge transfer among different RAC sizes are more suitable in this solvent.

The concentration of viologen in RAC monolayers, assuming that their thickness was equal to the particle diameter, was estimated by integrating the charge under the curve of a slow (5 mV/s) voltammogram (Figure S3.1). This estimation yielded 1.0 and 1.1 M for **RACs 1** and **2** respectively. This value is reasonable given that SEM and cross-sectional SEM analysis (Figure 2c-d and S3.1f) indicated a similar packing density for all monolayers, and only small distortions in particle shape upon contact with the electrode. Furthermore, and despite the uncertainties due to swelling in electrolyte, these concentrations are close to the theoretically-estimated 2M based on the density of viologens (1.25 g/cm^3)[25] and volume of the RAC particle.

The shape of the CV and square-root scan rate dependence of **RAC 1-3** films suggests a strong component of charge diffusion within the particles (Figure 2b, S3.1). Although RACs are immobilized on the surface, long-distance charge transfer from the electrode to the bulk particle film presents itself as a diffusive component. This phenomenon has been explained in terms of pendant-to-pendant charge hopping via the Dahms-Ruff relationship[26-27]:

$$D = D_{phys} + D_{CT} = D_{phys} + (1/6)k_{ex}\delta^2 C^* \quad (1)$$

Where D is the total diffusion coefficient for charge transfer, D_{phys} is related to the physical transport of redox species to the electrode, k_{ex} is the self-exchange rate constant for electron transfer between neighboring redox centers, δ is the distance between these, and C^* is their bulk concentration in the film. Because the particles are immobilized as a monolayer, D_{phys} is assumed to be negligible, while diffusive charge transport, D_{CT}, dominates the transient response.

Although Figure 2b evidenced a component of charge diffusion, the response was still within a regime where the current scaled with particle diameter. This suggested possible differences among the RAC sizes given that all other conditions (i.e. supporting electrolyte, solvent, and electrode area) were equal throughout. To explore these differences in diffusional transport, the RAC monolayer CVs were compared to simulations of a surface-confined film across the RAC sizes. Plausible concentrations of redox-active units were used to compare the

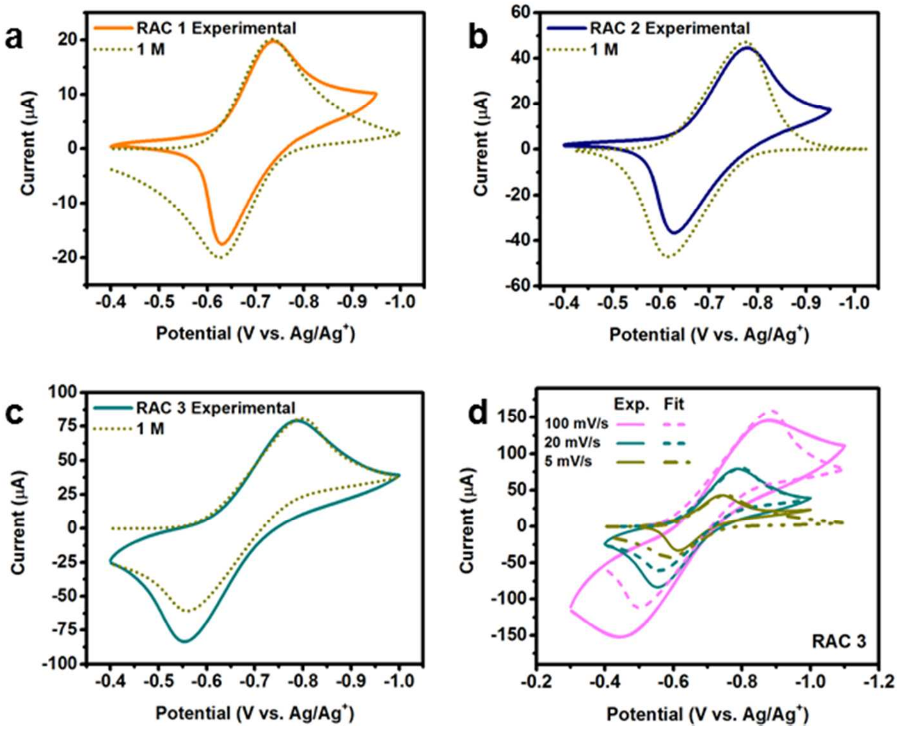

Figure 3. RAC Monolayer comparison to varying D_{CT} values. (a-c) All plots show experimental CV at 20 mV/s for each RAC compared to theoretical fits at 1 M with corresponding D_{CT} values shown in Table S3.1. **a. RAC 1 b. RAC 2 c. RAC 3 d.** Comparison of experimental (solid line) CVs for **RAC 3** compared to simulation (dash) using D_{CT} = 8.0× 10^{-11} cm^2/s at varying scan rates. In all CVs, an uncompensated resistance ~1 kΩ was observed and used in simulations.

experimental CVs and calculate a range of values for charge transfer diffusion coefficients (See Figure S3.2 for simulation parameters). Simulated CV curves indicate that D_{CT} values for all RACs lie within 10^{-11} – 10^{-12} cm^2/s when concentration (C*) is ≤ 2 M (Figure S3.2, Table S3.1). From the SEM cross analysis, thickness was assumed to be that of the dry RAC diameter due to the confined packing on the electrode surface. For **RACs 1-2**, changes in D_{CT} below 0.5 M do not give rise to a close fit regardless of the chosen value of D_{CT}. Figure 3 a-c shows plausible fits when assuming the film concentration of 1.0 M, close to the experimentally-obtained value. Thus, when considering monolayer RAC concentrations to range between 2.0 – 0.5 M, D_{CT} values are at a similar scale to reported viologen polymeric systems at 10^{-11} cm^2/s.[27] Interestingly D_{CT} also seemed to increase with RAC diameter, supporting that the observed trend in Figure 2b is due to charge transfer differences between the films. According to these results, larger **RAC 3** with a D_{CT} value of 8.0 × 10^{-11} cm^2/s (for 1 M) exhibits improved charge transfer properties, possibly arising from higher surface area exposed to electrolyte. Figure 3d shows that the calculated D_{CT} for **RAC 3** is in reasonable agreement with CV at various scan rates. Possible discrepancies with the model may arise from the assumption of linear diffusion within the monolayer films, although the analysis in Figure 3 serves as a reasonable point of comparison that might motivate further mechanistic studies.

SECM RAC Electrochemical Measurements To further explore the charge transfer properties of RACs at the nanoscale while minimizing IR drop effects, we performed scanning electrochemical microscopy (SECM) experiments. A glass substrate was prepared with a low loading of **RAC 3**. This substrate was then immersed into 0.1 M $LiBF_4$ in acetonitrile. A 300 nm radius SECM probe electrode was approached towards the glass substrate in an area that contained **RAC 3** (Figure S3.3a). Cyclic voltammetry exhibited two redox processes identified with the $V^{2+}/V^{\cdot+}$ and $V^{\cdot+}/V$ redox couples, where V is a viologen unit (Figure S3.3). Chronoamperometry under potential control allowed us to perform a reversible particle electrolysis for the $V^{2+}/V^{\cdot+}$ redox pair using the small contact area for the SECM tip. The cathodic steps show differences in charge observed with respect to the anodic step, which are likely due to small traces of O_2 in the cell. However, the fully reproducible anodic steps indicate that RACs can withstand current densities of 0.2 A/cm^2 (based on electrode area) when potentiometrically discharged (Figure S3.3). The limiting charge observed in this experiment corresponded to 3.5 nC. When compared to theoretical values of 2 M per individual RAC, it is possible that the SECM electrode was addressing more than one RAC. Nonetheless, the electrolysis allowed for the observation of high current density capabilities at the nanoscale, as well as reversible charge and discharge.

Electrochemical Reactivity of Dispersed RACs 1-3. To further probe the efficiency and rate of charge/discharge processes, we prepared dispersions of varying particle size (**RACs 1-3**) in acetonitrile. Their electrochemical properties were first studied with CV under static conditions at an equivalent viologen concentration of 10 mM. Studies using a macro disk electrode revealed quasi-Nernstian response with signatures that suggest chemical and electrochemical reversibility (Figure 4a). The first redox process showed peak current ratios near unity centered at E^o= -0.7 V vs. Ag/Ag^+ (0.1 M

$AgNO_3$), consistent with the voltammetry of the monomer unit.[12] Scan rate dependence analysis of the CV peak height did not conclusively show a strong correlation vs. υ or $\upsilon^{1/2}$, suggesting that the CVs are neither described by pure diffusion-limited mass transfer nor that expected for a surface-confined electroactive film (Figure 4a, Figure S3.4). It is likely that both processes occur simultaneously, as observed for soluble redox active

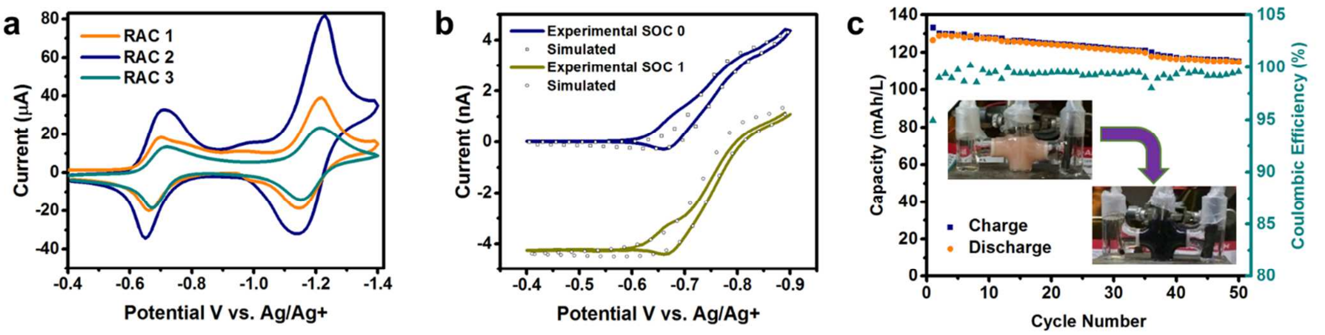

Figure 4. Dispersion-phase electrochemical properties of RACs 1-3. a. Cyclic voltammograms of **RACs 1-3** on 0.03 cm^2 Pt disk electrode (ν = 75 mV/s, 10 mM). **b.** Microelectrode voltammetry of RAC **2** at neutral and charged state as compared to simulation with D = 4.8×10^{-7} cm^2/s, E^o = -0. 73 V, k^o = 0.015 cm/s, α = 0.5. Microelectrode radius was 12.5 µm and concentration of redox species was 15 mM. **c.** Charge/Discharge performance of **RAC 2** bulk electrolysis on SGL GFA6 carbon electrode. Theoretical capacity is 134 mAh/L (5 mM). Inset: Visual changes are observed from neutral (top, SOC: 0) to charged state (bottom, SOC: 1). All dispersions were prepared in 0.1 M $LiBF_4$ in acetonitrile.

polymers (RAPs).[12, 26, 28] In both RACs and RAPs, a persistently adsorbed layer of redox material likely mediates electron transfer to the solution species through interparticle interactions. Likewise it is expected that dispersed individual RACs exchange charge within the diffusion layer. While a full description of this complex interplay is beyond the scope of this study, it is convenient to decouple contributions from film and solution species. The film contribution to the voltammetric signal was studied by performing CV on an electrode previously run in RAC dispersion. Once voltammetry was done in dispersion, the working electrode was thoroughly rinsed, dried and placed in a blank electrolyte solution (Figure S3.5). The viologen RAC emerged film was electroactive and did not appear to impede the charge transfer to RACs within the potential of the first redox process when tested in blank electrolyte, confirming the formation of an adsorbed layer and its mediation of electron transfer. We did find, however, that excursions to potentials where the second electron process occurs, results in electrode fouling.[12] We therefore focused solely on the first electron transfer. Importantly, we found that each of the viologen RAC dispersions were redox- active and, at equivalent pendant concentration, they displayed voltammetric signatures within the same order of magnitude in current intensities independent of their particle size (Figure 4a). The only difference we did observe between particle sizes is that **RAC 3** consistently exhibited lower current levels than **RACs 1-2**. We ascribe this suppression in current levels to the stabilizer used for **RAC 3** (Figure S3.5, Table S3.1). This stabilizer may affect the arrangement of RACs on the electrode surface, in turn affecting the current response in multi-layer films.

Microelectrode cyclic voltammetry (ME CV) displayed a steady-state profile resulting from reaction and physical transport of RACs to the electrode surface (Figure 4b). The microelectrode response showed signatures from both adsorption (as a pre-peak) and expected radial diffusion.[29] The wave shape from the ME CV measurements was compared to theoretical fits of Nernstian reactions to shed light on kinetic complications that could be expected on solution species showing similar wave slopes. The model fit is only taken as an approximation since it does not account for adsorption, mediation of the adsorbed film to solution species, or interparticle charge exchange in the solution phase. However, comparison to a continuum model of CV provides a suitable baseline for contrasting the behavior of RACs to that of small molecules. Nevertheless, fitting of ME CVs to theory showed that electron transfer to the solution species, although not yielding a fully Nernstian response, is fast~~,~~ with an estimated comparable standard electrochemical rate constant k^o = 0.015 cm/s. We assumed chemical reversibility, as observed in macrodisk CV and a transfer coefficient α of 0.5. Broadening of the ME CV wave and the incipient second viologen reduction wave causes the observation of only a narrow steady state plateau. The fitting of this wave helped in obtaining transport parameters. The apparent diffusion coefficient, D, obtained from steady-state ME CV was calculated using the steady state current, expressed as $i_{ss} = 4nFaDC^*$, where n is assumed to be 1, F is Faraday's constant, a is the radius of the electrode equal to 12.5 µm, and C* is the bulk equivalent concentration of pendants in the RAC. Apparent values of D were found to be 1.7×10^{-7} cm^2/s, 4.8×10^{-7} cm^2/s, and 1.8×10^{-7} cm^2/s for **RACs 1-3** respectively. We notice, however, that small differences in D between **RACs 1-3** do not scale as expected from the Einstein-Stokes relationship, implying that D possibly reflects other contributions in charge transport[30], including that from D_{CT}. This observation is not unreasonable considering their size; for example, in the case of **RAC 3** its swollen diameter is 5% of the microelectrode diameter. For comparison, dynamic light scattering (DLS) experiments showed D values of 7.38×10^{-8} cm^2/s, 5.46×10^{-8} cm^2/s, 0.927×10^{-8} cm^2/s for **RACs 1-3** respectively, where consistently the electrochemical estimate was higher than that of DLS. An interesting manifestation of the impact of RAC interactions with electrodes was that CV experiments in dispersion showed lower currents than those observed on emerged RAC films on such electrodes (Figure S3.5). To explore this voltammetric response, increasing amounts of **RAC 2** were loaded onto a Pt disk electrode by dropcasting and a chronoamperometric step was applied to measure the film's charge. As the RAC loading increased, the charge followed up to a saturation point, wherein afterwards the measured current and charge decreased (Figure S3.7). This behavior is possibly due to insufficient diffusion of supporting electrolyte to the electrode surface. These results suggest that when in dispersion, RACs form a compact multi-layer arrangement on the electrode surface that decreases slightly the current.

Bulk Charge Storage Properties of RACs Despite their large size, dispersed RACs collect and store charge efficiently from a stationary electrode in bulk dispersions. To explore the charge storage capacity and stability of viologen-RACs, inert-atmosphere, potential-controlled bulk electrolysis (BE) and ME CV were performed on all the particle sizes to a state of charge (SOC) of unity. Mirroring the experiments with a single RAC particle, BE unambiguously demonstrated that charge injection during electrolysis occurred efficiently on the solution species. Figure 4b-c shows the BE and steady state voltammetry of **RAC 2.** These particles showed the most reversible cycling and displayed access to 91 ± 3% of the theoretically-accessible groups over fifty full cycles with a Coulombic efficiency of 99 ± 1% (Figure 4c, Figure S3.7). Only slight decreases in capacity access were observed over time (< 10% after 50 cycles), possibly due to side-product contamination from the counter electrode compartment or RAC adsorption on glass frits. ME CV in all cases confirmed chemically-reversible transformation from V^{2+} to $V\cdot^{+}$ as shown in Figure 4b for **RAC 2** after the full electrolysis.

To further support dispersion-phase studies, the structural and chemical stability of RACs in the charged state ($V\cdot^{+}$, SOC: 1) and after multiple charge/discharge cycles (V^{2+}, SOC: 0) were studied using UV-vis, dynamic light scattering (DLS), and ex-situ SEM. Full reduction of **RACs 1-3** was achieved by BE at an overpotential of -150 mV. UV-vis absorbance spectra shows distinct peaks for the reduced state of viologen RACs at the 370 and 540 nm regions as opposed to the neutral state, which absorbs ca. 260 nm. This reduced state in **RACs 1-3** was stable for at least 7 days with only a minor decrease of less than 9 % in absorbance over this time (Figure 5, and S3.8). The structural stability of the RACs was determined by characterizing the size of the particles after a charging step. DLS analysis shows that the size of the charged RACs increased by approximately 20 nm as compared to their original state, although the increment was within the standard deviation of the measurements (Table S2.3). SEM and DLS analysis of RACs after multiple charge/discharge BE cycles indicate that the size and shape of the particles is maintained (Figure S3.10, Table S2.3).

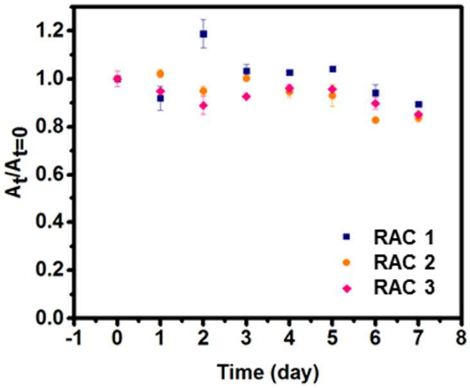

Figure 5. Time dependent stability of RAC reduced state. UV-vis absorbance at 370nm normalized to the initial value over time of the reduced RACs to quantify chemical stability of their reduced state.

Size Exclusion of RACs in Porous Separators Given the excellent prospects for the use of RACs as storage media, we explored them as "zero" crossover nano-materials for size-exclusion flow batteries. The use of RACs in combination with a nanoporous separator dramatically decreased crossover. All three **RACs 1-3** at an equivalent viologen concentration of 10 mM showed negligible crossover within the limit of detection across both Celgard 2325 (pore diameter 28 nm) and Celgard 2400 (pore diameter 43 nm, Table S4.1). In great contrast, $LiBF_4$, the supporting electrolyte used in our experiments, freely crossed the separator. Compared to our previous study[12] on redox active polymers, this a great improvement in material rejection across Celgard 2325. In that case, the largest polymer was rejected 86 % while RACs are rejected by >99 %. Additionally, size-dependent rheological studies of RAC dispersions in electrolyte media (Figure S4.1) revealed that larger RAC sizes show exciting prospects for maximizing the energy density[31] of the electrolyte while keeping the viscosity low enough for reliable flow operation[32-34] even at high concentrations up to 40 wt%. As expected, dispersions composed of smaller sized RACs exhibited higher viscosity than ones of larger sized RACs at identical concentrations (Figure 6, S4.1). Thus, larger RACs display better prospects for flow while increasing size-selectivity.

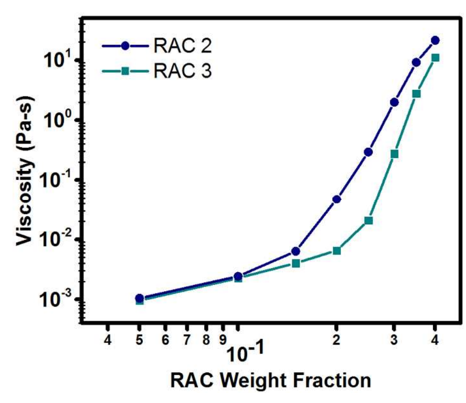

Figure 6. Rheological properties of RACs. Apparent viscosity measured at 100 s^{-1} of viologen dispersions of varying particle size and weight fraction in acetonitrile with 1 M $LiBF_4$.

Prototype NRFB Explorations Since crossover and rheological experiments showed encouraging results, prototype size-exclusion NRFB experiments were conducted as a proof of concept. To demonstrate the facility of RAC modular synthesis, we functionalized x**PVBC** particles with a ferrocene monomer to generate catholyte RACs (**RAC 4**, Table S2.5). SEM showed **RAC 4** to be 88 ± 11 nm in dry diameter and electrochemical characterization demonstrated reversible activity (Figure S4.2). A prototype flow cell was assembled using RACs of similar diameters, **RACs 2** and **4**, as the redox active species in the anolyte and catholyte compartments, respectively (Figure 7). A commercially available porous membrane (Celgard 2325) was used as the separator between compartments. Low concentrations (10 mM, 0.74 wt %) were used to test the initial concept if an all-RAC flow cell is a viable concept for RAC energy storage applications. Taking into account the low concentration, low current densities were chosen as to prevent polarization losses. The operating cell revealed high reversibility with an average coulombic efficiency of 94 ± 4 % over 11 cycles at C/20 (43 μA/cm^2) and volumetric flow of 5 mL/min. Electrochemical performance of the cell was tracked by energy and voltage efficiencies, which were highly stable and above 90 % (Figure 7, S4.3). Even though the experimental conditions apply current densities in the micro-scale, the resulting

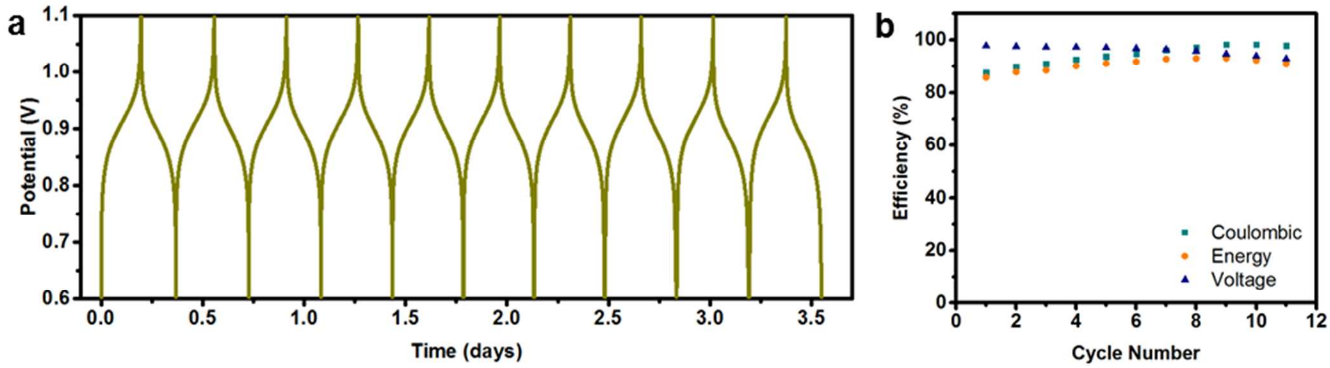

Figure 7. Performance of RACs as flow cell active material. a. RAC 2/RAC 4 flow battery cell charge/discharge profile over time cycling at C/20 (43 μA/cm^2) and linear flow of 5 mL/min (10mM, 15mL in 0.1 M $LiBF_4$ in acetonitrile). **b. RAC 2/RAC 4** flow battery cell response in terms of efficiency for 11 cycles of galvanostatic cycling.

metrics of the NRFB are comparable to that of some organometallic complexes,[35] organic small molecules[36] and macromolecular designs such as polymers.[14] Additionally, RACs offer the advantage of negligible crossover.

Flow cell testing for over 3.5 consecutive days highlights the robustness and stability displayed by these particles. Capacity retention remained stable at 55 ± 1 mAh/L over the 11 cycles.

Nevertheless, it should be noted that capacity access was low at 21 % of theoretical capacity (268 mAh/L at 10 mM). This low accessibility is likely from a combination of low loading and observed sedimentation from **RAC 4** (Figure S4.3). This is the first example of an all RAC NRFB, thus optimization will be required to fully make use of the billions of redox active units within RACs, but this prototype demonstrates a possible application for RACs as size-exclusion materials.

CONCLUSIONS

In summary, we have synthesized and characterized the electrochemical performance of redox active colloids. These stable, well-dispersed energy storage systems are composed of sub-micron particles that exhibit near-zero crossover. As demonstrated, RACs can be implemented in size-selective energy applications in the form of individual particles, monolayer films, and bulk dispersions. Their combination of surface-confined and diffusion-limited behavior gives rise to efficient charge transport in solution in each of these motifs. Their performance in a simple flow battery cell was also investigated. The observed coulombic, energy and voltage efficiencies revealed that RACs can cycle reversibly in this configuration. Due to the modular nature of RAC synthesis, this paradigm can be expanded to explore diverse families of anolyte and catholyte pendant moieties. Because they are new materials, significant rheological, electrode and design improvements are emerging from our laboratories to maximize their potential. Given their broad versatility, RACs offer considerable promise for emerging applications in energy storage whether it be as individual particles, adsorbed films or in dispersion-phase.

ASSOCIATED CONTENT

Supporting Information

Experimental methods and supplementary figures and tables. This material is available free of charge via the Internet at http://pubs.acs.org.

AUTHOR INFORMATION

Corresponding Author

*jsmoore@illinois.edu, *joaquinr@illinois.edu

Author Contributions

‡These authors contributed equally.

Notes

The authors declare no competing financial interests.

ACKNOWLEDGMENT

This work was supported as part of the Joint Center for Energy Storage Research (JCESR), an Energy Innovation Hub funded by the U.S. Department of Energy, Office of Science, Basic Energy Sciences. M. B. acknowledges support by the National Science Foundation Graduate Research Fellowship Program under Grant No. DGE-1144245. K.H.B. gratefully acknowledges the Arnold and Mabel Beckman Foundation for a Beckman Institute Postdoctoral Fellowship. J.R.L. acknowledges additional support from the Alfred P. Sloan Research Foundation. Sample characterization was carried out in part in the Frederick Seitz Materials Research Laboratory Central Research Facilities and the Beckman Institute for Advanced Science and Technology, University of Illinois; we acknowledge the JCESR Flow Chemistry Sprint team's efforts in the development of the "prototyping everywhere" cell (Gen 1 Cell) used in this work; Qu Subing for assistance with DLS. We would like to thank Celgard and SGL Group for samples.

REFERENCES

1. Wang, Y.; He, P.; Zhou, H., *Adv. Energy Mater.* **2012,** *2*, 770.
2. Jia, C.; Liu, J.; Yan, C., *J. Power Sources* **2010,** *195*, 4380.
3. Darling, R.; Gallagher, K.; Xie, W.; Su, L.; Brushett, F., *J. Electrochem. Soc.* **2016,** *163*, A5029.
4. Song, Z.; Zhou, H., *Energy Environ. Sci.* **2013,** *6*, 2280.
5. Zhou, X. F.; Cheng, W.; Compton, R. G., *Nanoscale* **2014,** *6*, 6873.
6. Cheng, W.; Batchelor-McAuley, C.; Compton, R. G., *Chemelectrochem* **2014,** *1*, 714.
7. Astruc, D., *Nat. Chem.* **2012,** *4*, 255.
8. Amatore, C.; Bouret, Y.; Maisonhaute, E.; Goldsmith, J. I.; Abruña, H. D., *Chem. Eur. J.* **2001,** *7*, 2206.
9. Zu, X.; Rusling, J. F., *Langmuir* **1997,** *13*, 3693.
10. Phillip, W. A.; Amendt, M.; O'Neill, B.; Chen, L.; Hillmyer, M. A.; Cussler, E. L., *ACS Appl. Mater. Interfaces* **2009,** *1*, 472.
11. Liang, Y.; Tao, Z.; Chen, J., *Adv. Energy Mater.* **2012,** *2*, 742.
12. Nagarjuna, G.; Hui, J. S.; Cheng, K. J.; Lichtenstein, T.; Shen, M.; Moore, J. S.; Rodriguez-Lopez, J., *J. Am. Chem. Soc.* **2014,** *136*, 16309.
13. Janoschka, T.; Martin, N.; Martin, U.; Friebe, C.; Morgenstern, S.; Hiller, H.; Hager, M. D.; Schubert, U. S., *Nature* **2015,** *527*, 78.
14. Winsberg, J.; Hagemann, T.; Muench, S.; Friebe, C.; Häupler, B.; Janoschka, T.; Morgenstern, S.; Hager, M. D.; Schubert, U. S., *Chem. Mater.* **2016,** *28*, 3401.
15. Alotto, P.; Guarnieri, M.; Moro, F., *Renew. Sust. Energ. Rev.* **2014,** *29*, 325.
16. Darling, R. M.; Gallagher, K. G.; Kowalski, J. A.; Ha, S.; Brushett, F. R., *Energy Environ. Sci.* **2014,** *7*, 3459.
17. Shin, S.-H.; Yun, S.-H.; Moon, S.-H., *RSC Adv.* **2013,** *3*, 9095.
18. Lin, K. X.; Chen, Q.; Gerhardt, M. R.; Tong, L. C.; Kim, S. B.; Eisenach, L.; Valle, A. W.; Hardee, D.; Gordon, R. G.; Aziz, M. J.; Marshak, M. P., *Science* **2015,** *349*, 1529.
19. Brushett, F. R.; Vaughey, J. T.; Jansen, A. N., *Adv. Energy Mater.* **2012,** *2*, 1390.
20. Leung, P.; Li, X.; Ponce de Leon, C.; Berlouis, L.; Low, C. T. J.; Walsh, F. C., *RSC Adv.* **2012,** *2*, 10125.
21. Wang, W.; Luo, Q. T.; Li, B.; Wei, X. L.; Li, L. Y.; Yang, Z. G., *Adv Funct Mater* **2013,** *23*, 970.
22. Chonde, Y.; Liu, L. J.; Krieger, I. M., *J. App. Polym. Sci.* **1980,** *25*, 2407.
23. Margel, S.; Nov, E.; Fisher, I., *J. Polym. Sci. A Polym. Chem.* **1991,** *29*, 347.
24. Druta, I.; Avram, E.; Cozan, V., *Eur. Polym. J.* **2000,** *36*, 221.
25. CRC Handbook of Pesticides. Milne, G. W. A., Ed. CRC Press: Boca Raton, 1995.
26. Burgess, M.; Hernandez-Burgos, K.; Simpson, B. H.; Lichtenstein, T.; Avetian, S.; Gavvalapalli, N.; Cheng, K.; Moore, J. S.; Rodriguez-Lopez, J., *J. Electrochem. Soc.* **2015,** *163*, H3006.
27. Dalton, E. F.; Murray, R. W., *J. Phys. Chem.* **1991,** *95*, 6383.
28. Peerce, P. J.; Bard, A. J., *J. Electroanal. Chem. Interfacial Electrochem.* **1980,** *114*, 89.
29. Bard, A. J.; Faulkner, L. R., *Electrochemical Methods: Fundamentals and Applications*. 2nd ed.; Wiley: 2000.
30. Paulson, S. C.; Okerlund, N. D.; White, H. S., *Anal. Chem.* **1996,** *68*, 581.
31. Desmond, K. W.; Weeks, E. R., *Phys. Rev. E* **2014,** 90.
32. Wei, T.-S.; Fan, F. Y.; Helal, A.; Smith, K. C.; McKinley, G. H.; Chiang, Y.-M.; Lewis, J. A., *Adv. Energy Mater.* **2015,** 5.
33. Smith, K. C.; Chiang, Y.-M.; Carter, W. C., *J. Electrochem. Soc.* **2014,** *161*, A486.
34. Saunders, F. L., *J. Colloid Sci.* **1961,** *16*, 13.
35. Xing, X.; Zhao, Y.; Li, Y., *J. Power Sources* **2015,** *293*, 778.
36. Wei, X.; Xu, W.; Huang, J.; Zhang, L.; Walter, E.; Lawrence , C.; Vijayakumar, M.; Henderson, W. A.; Liu, T.; Cosimbescu, L.; Li, B.; Sprenkle, V.; Wang, W., *Angew. Chem. Int. Ed.* **2015,** *54*, 8684.